Scilight

Highlights in High-Energy Physics
https://www.sciltp.com/journals/hihep

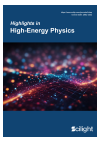

Article

Tau Lepton Reconstruction at the Muon Collider: Cross Section Measurement of the $H \to \tau^+\tau^-$ Process

Kevin Dewyspelaere, Giacomo Da Molin, Giovanni Battista Marozzo, Lorenzo Valla † and Michele Gallinaro *

Laboratório de Instrumentação e Física Experimental de Partículas, 1649-003 Lisbon, Portugal
* Correspondence: michele.gallinaro@cern.ch
† Current address: Marietta-Blau-Institut für Teilchenphysik der Österreichischen Akademie der Wissenschaften, 1050 Wien, Austria.

How To Cite: Dewyspelaere, K.; Da Molin, G.; Marozzo, G.B.; et al. Tau Lepton Reconstruction at the Muon Collider: Cross Section Measurement of the $H \to \tau^+\tau^-$ Process. *Highlights in High-Energy Physics* **2026**, *2*(1), 3. https://doi.org/10.53941/hihep.2026.100003

Received: 23 January 2026
Revised: 18 March 2026
Accepted: 24 March 2026
Published: 31 March 2026

Abstract: Studies of Higgs boson properties are crucial for the understanding of the standard model (SM), as the Higgs boson could couple to new particles and provide hints of physics beyond the SM (BSM). Among the proposed future colliders, the Muon Collider would allow unprecedented precision measurements of Higgs boson parameters. The goal of this study is to estimate the statistical uncertainty on the cross section of the $H \to \tau^+\tau^-$ process at a center-of-mass energy of 10 TeV. Tau leptons are reconstructed using the `TauFinder` algorithm. The efficiency of hadronic τ (τ_h) identification is found to be above 80% for 1-prong and about 50% for 3-prong decay modes. This study focuses on the fully hadronic final state of the $H \to \tau^+\tau^-$ decay. The main background processes are discussed and compared to the signal. The visible invariant mass is reconstructed and template fits are performed using Monte Carlo toy experiments. For an integrated luminosity of 10 ab^{-1} a relative statistical uncertainty on the signal cross section of $\Delta\sigma/\sigma = 1.3\%$ is obtained, reduced to 0.9% when two interaction points are assumed. Comparisons with sensitivities at other future colliders are also presented, and possible improvements to the analysis are discussed.

Keywords: muon collider; future colliders; Higgs; Tau physics

1. Introduction

1.1. The Higgs Physics and Prospects for Future Colliders

The Higgs boson (H), a key component of the Standard Model (SM), is a scalar neutral particle introduced by the Brout–Englert–Higgs mechanism [1]. It was first observed in 2012 by the ATLAS [2] and CMS [3] collaborations at the LHC. Its properties, including couplings, decay modes and mass, have been extensively studied, showing consistency with SM predictions, though precision is still limited for many channels. Key open questions remain, such as the measurement of Higgs self-couplings and the search for possible decays into beyond-the-SM (BSM) particles, including dark matter.

To address these challenges, future collider projects, such as the HL-LHC [4], FCC [5], CEPC [6], ILC [7], CLIC [8], and Muon Collider [9], aim at producing Higgs bosons in unprecedented numbers and explore the properties with higher precision. These facilities will significantly improve sensitivity to Higgs couplings, in particular to τ leptons, and will probe Higgs self-interactions, offering unique opportunities to uncover possible deviations from the SM and explore the possible presence of new physics processes.

1.2. The Muon Collider Project

The Muon Collider (MuCol) [9] represents a unique proposal among future colliders, as it would collide muons and antimuons rather than protons or electrons. Thanks to the large muon mass, synchrotron radiation is strongly suppressed, allowing multi-TeV collisions in a relatively compact ring, while retaining the clean leptonic environment typical of e^+e^- machines. This makes the MuCol simultaneously a precision tool and a high-energy

frontier collider. Its physics potential is particularly strong in the Higgs sector. At multi-TeV energies, Higgs boson production is dominated by vector boson fusion (VBF) and Higgs-strahlung, enabling precise measurements of Higgs couplings and self-interactions with large statistics.

Figure 1 illustrates the conceptual scheme of the facility as designed by the International Muon Collider Collaboration (IMCC), which foresees staged operation at 3 TeV and 10 TeV, with luminosities sufficient to produce hundreds of thousands of Higgs bosons per year. Despite its advantages, the MuCol also faces major technological challenges, including production, cooling, and rapid acceleration of short-lived muon beams, as well as the mitigation of the beam-induced background (BIB), originating from muon decays along the beamline that produce a large flux of secondary particles entering the detector. Nevertheless, its capability to combine energy reach with precision measurements makes it one of the most promising projects for exploring the Higgs sector and possible physics beyond the SM.

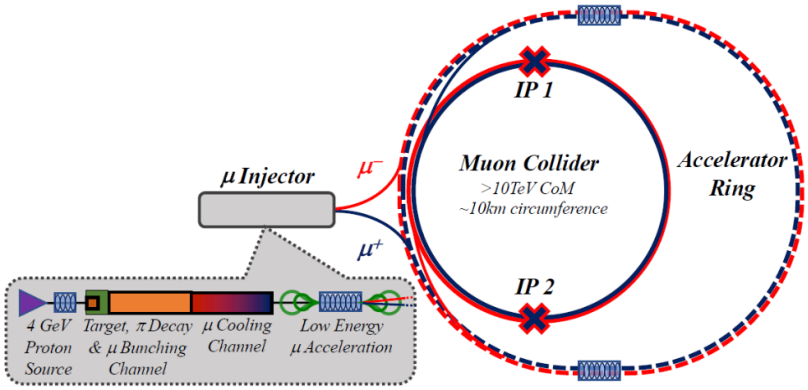

Figure 1. Conceptual scheme of the MuCol facility as planned by the International Muon Collider Collaboration (IMCC). (from Ref. [10]).

2. Simulation and Event Reconstruction

2.1. The MAIA Detector Apparatus

The MAIA (Muon Accelerator Instrumented Apparatus) detector [11] is a new concept specifically designed for $\sqrt{s}$=10 TeV $\mu^+\mu^-$ collisions, aiming to cope with the unique challenges of a high-energy muon collider. The layout combines an all-silicon tracker embedded in a 5 T solenoidal field, surrounded by high-granularity calorimeters: a silicon–tungsten electromagnetic calorimeter (ECAL) and an iron–scintillator hadronic calorimeter (HCAL), optimized for particle-flow reconstruction. The outermost layer consists of an air-gap muon spectrometer, enabling precise standalone tracking of high-momentum muons (Figure 2).

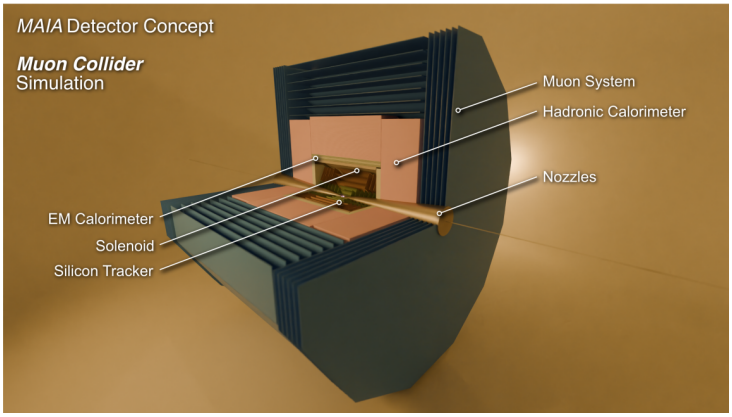

Figure 2. Illustration of the MAIA detector layout. The detector is shown with a $\pi/2$ cutaway in ϕ for illustration (from Ref. [11]).

A key feature of the apparatus is its capability to operate under intense BIB from muon decays. Overall, MAIA is conceived as a general-purpose detector for the Muon Collider, providing both the hermeticity and precision required for Higgs and SM measurements, as well as sensitivity to new physics phenomena [12].

2.2. Event Reconstruction

The reconstruction of physics objects at the Muon Collider is performed with a dedicated simulation, which proceeds from event generation to the creation of particle flow (PF) objects ready for analysis. Signal events are generated with external event generator tools such as MadGraph5 [13] with Pythia8 that is used for τ decay, hadronization and showering, and then passed through a full detector simulation based on GEANT4 [14] within the ILCSoftware [15] framework adapted for MuCol [16]. Digitization modules implemented in MARLIN [17] convert simulated energy deposits into detector hits, applying realistic spatial and timing resolutions. In this study, BIB is not considered and only single interactions are included.

The calorimetric information is processed with the Pandora Particle Flow Algorithm (PandoraPFA) [18], which combines tracker and calorimeter data to reconstruct individual particles with optimal precision. The individual particles, i.e., PF objects, are then produced by associating tracks and clusters, assigning particle identities and preparing the reconstructed objects for physics analyses.

This reconstruction chain provides a realistic modeling of the detector response, except for the BIB which is not included in this study.

3. Tau Reconstruction and Identification

3.1. Tau Lepton in the Standard Model

The τ lepton is a third-generation fermion, and in the SM τ pairs can be produced in the decays of electroweak bosons, such as $H \to \tau^+\tau^-$, $Z \to \tau^+\tau^-$.

The τ lepton is unstable, with a short lifetime of about 2.9×10^{-13} s [19], and decays via the weak interaction into a ν_τ and a virtual W boson. The subsequent W boson decays either to a purely leptonic final state (τ_ℓ) or to a hadronic final state (τ_h), as illustrated in Figure 3.

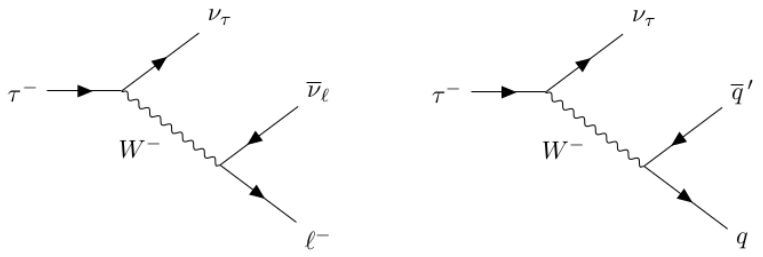

Figure 3. Feynman diagrams for a τ^- lepton decaying into leptonic (**left**) and hadronic (**right**) final states.

In the hadronic final state, the visible decay products are mostly light mesons ($\pi^\pm$, $K^\pm$, π^0), which result in one or three charged hadrons in the final state. This motivates the classification into 1-prong and 3-prong categories.

The main SM decay modes of the τ lepton, together with their branching fractions, are summarized in Table 1. Roughly 35% of τ decays are purely leptonic, while the remaining 65% are hadronic, making hadronic τ reconstruction a key experimental challenge.

Table 1. Decays of τ leptons and their branching fractions [20]. Decay modes with intermediate resonances are shown in the middle column. Charged hadrons are denoted by $h^\pm$.

Decay Mode	Meson Resonance	$\mathcal{B}$ [%]
$e\nu_e\nu_\tau$		17.8
$\mu\nu_\mu\nu_\tau$		17.4
all leptonic decays		**35.2**
$h^\pm\nu_\tau$		11.5
$h^\pm\pi^0\nu_\tau$	$\rho(770)$	26.0
$h^\pm\pi^0\pi^0\nu_\tau$	$a_1(1260)$	9.5
$h^\pm h^\mp h^\pm\nu_\tau$	$a_1(1260)$	9.8
$h^\pm h^\mp h^\pm\pi^0\nu_\tau$		4.8
other hadronic decays		3.2
all hadronic decays		**64.8**

3.2. The `TauFinder` *Algorithm*

`TauFinder` [21] was originally developed for τ reconstruction in the CLIC experiment and is therefore optimized for lepton collider environments. It follows a cone-based jet-finding approach, using the four-momenta of charged and neutral reconstructed particles. The algorithm starts by selecting high-energy charged particles as seeds and builds a τ candidate by iteratively adding other charged and neutral particles within a narrow "signal" cone of radius $\Delta R = 0.10$ around the seed direction, dynamically updating the cone axis. The cone size is defined as $\Delta R = \sqrt{(\Delta\eta)^2 + (\Delta\phi)^2}$, where $\Delta\eta$ and $\Delta\phi$ are the differences of pseudo-rapidities and azimuthal angles. Once all candidates are reconstructed, a merging step ensures that overlapping objects are combined.

To reduce misidentification, `TauFinder` applies a few quality cuts: the number of charged tracks must be either one or three (reflecting 1-prong and 3-prong τ decays), the total number of particles from τ decays must be below ten, and the reconstructed candidate charge must be ± 1. Additional reconstruction and isolation criteria are used to further suppress background: seeds must have transverse momentum $p_T > 5$ GeV, all associated particles $p_T > 1$ GeV, and an "isolation" cone ($0.10 < \Delta R < 0.40$) is built around the τ candidate.

Candidates passing all requirements are identified as reconstructed τ leptons, with the charge distinguishing τ^+ from τ^-. A study of the τ isolation and its use to reject jets faking τs is presented in Section 3.4.

3.3. `TauFinder` *Algorithm Performance*

The performance of the `TauFinder` algorithm was evaluated using a sample of 15,000 τ "particle-gun" (τ-gun) events, equally split between τ^+ and τ^-. The generated τs were assigned kinematical properties uniformly distributed in $p_T \in [20, 320]$ GeV, $\phi \in [0, 2\pi]$, $\theta \in [10°, 170°]$. In the "particle-gun" sample, the τ decay is handled directly by GEANT4 during the detector simulation, after the generation step.

`TauFinder` does not distinguish between hadronic (τ_h) and leptonic (τ_ℓ) decays at the reconstruction level; a basic classification can be introduced by requiring the presence of charged hadrons among the decay products. In addition, the current framework does not reconstruct neutral pions explicitly, and photon objects are used instead. The classification of reconstructed τ_h was therefore performed only by prong multiplicity, i.e., counting the number of charged pions associated with each candidate.

In this study, only hadronic τ decays were selected to evaluate the reconstruction efficiency.

Figure 4 shows the resulting efficiency as a function of the generated visible transverse momentum p_T^{vis}, for both 1-prong and 3-prong τ decays. No isolation requirement is applied in this efficiency study. The results indicate that 1-prong τ decays are reconstructed with an efficiency close to 80–90% over most of the p_T^{vis} range, only slightly below the pion reconstruction baseline due to the additional cuts imposed by `TauFinder`. In contrast, 3-prong τ decays exhibit a significantly lower efficiency, around 50–60%, with a mild dependence on p_T^{vis}. This reduction reflects the intrinsic challenge of reconstructing three charged prongs simultaneously, given the pion identification efficiency and the isolation requirements of the algorithm. Overall, these results confirm that `TauFinder` provides a robust reconstruction of 1-prong τ_h candidates, while highlighting the need for further optimization to improve the efficiency for 3-prong modes.

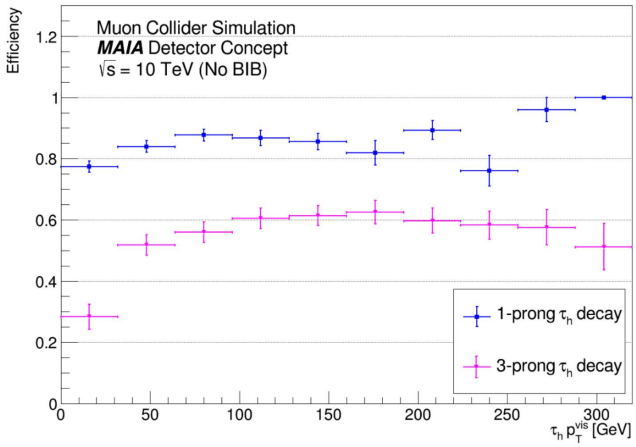

Figure 4. Reconstruction efficiencies of 1-prong and 3-prong τ decays with the `TauFinder` algorithm, as a function of the generated visible transverse momentum of the τ lepton. Results are shown for Muon Collider simulations with the MAIA detector concept at $\sqrt{s} = 10$ TeV. The beam induced background (BIB) is not included.

3.4. Tau Misidentification

In the context of τ lepton reconstruction and identification, an important aspect is the misidentification rate, i.e., the probability that a physics object that is not a τ lepton (for instance, a genuine hadronic jet or an electron) is incorrectly reconstructed as a τ candidate. Such objects, also referred to as fake τ, represent a potential source of background contamination in precision measurements such as the $H \to \tau^+\tau^-$ decay. In this study, particular attention is given to the misidentification of hadronic τ candidates reconstructed by `TauFinder`.

3.4.1. Rejection against Electrons

It was observed that many τ leptons in the electron decay mode ($\tau \to e\nu_e\nu_\tau$) at generator level were reconstructed as one-prong hadronic τ candidates. This effect can be seen in Figure 5, where the decay mode matrix shows a significant population in the "other" category at generator level but is reconstructed as 1-prong τ_h either as 1P0N (no neutrals) or 1P+N (with neutrals).

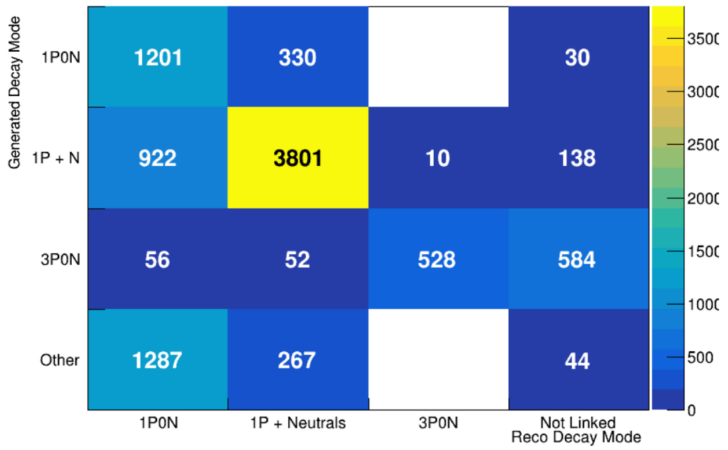

Figure 5. Decay mode matrix before the HCAL cut. A significant contamination of generator-level electron decays (included in the "Other" category in the y-axis) is reconstructed as 1-prong hadronic τ decays, either as 1P0N (no neutrals) or 1P+N (with neutrals); after the HCAL cut, yields are largely suppressed (Figure 6).

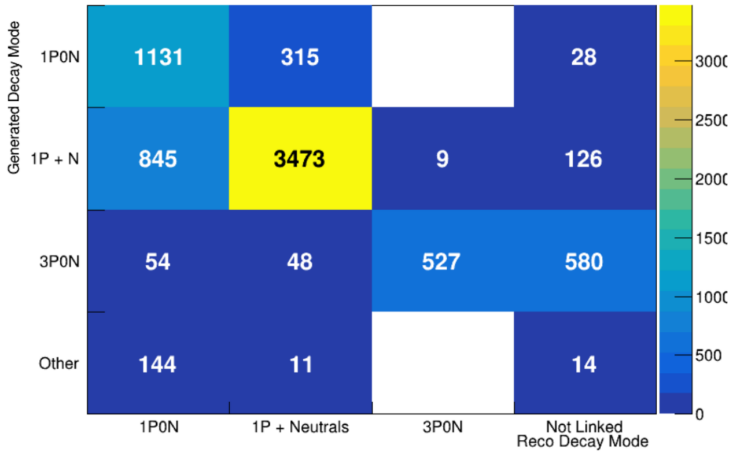

Figure 6. Decay mode matrix after the HCAL cut. The contamination from generator-level electrons reconstructed as hadronic τ's is largely removed.

To understand this misclassification, the electromagnetic fraction (EMF) associated to the τ_h energy cluster deposited in the ECAL and HCAL calorimeters was studied:

$$\mathrm{EMF} = \frac{E_{\mathrm{ECAL}}}{E_{\mathrm{ECAL}} + E_{\mathrm{HCAL}}}. \tag{1}$$

As expected, electrons peak at EMF = 1, since they deposit most of their energy in the ECAL. About 20% of reconstructed hadronic τ candidates also appear at EMF = 1; a large fraction of these are τ leptons in the electron decay mode misidentified as one-prong hadronic τs.

To mitigate this effect, at least some energy deposit in the HCAL is required. As shown in Figure 6, this cut removes the vast majority of events from the "other" category at generator level reconstructed as 1P0N or 1P+N, thus significantly improving the purity of the hadronic τ selection while keeping a high efficiency for genuine hadronic τ decays. After this cut, the probability that an electron is misidentified as a τ_h is approximately 2%. This cut is applied as a simple patch to remove misidentified electrons and further improvements in the pion and electron ID are certainly necessary.

3.4.2. Rejection against Jets

To quantify the fake τ_h rates, dedicated event samples were generated with MadGraph5 at leading order (LO): VBF $Z(\rightarrow q\bar{q})$ (light-flavor jets, 15k events), VBF $Z(\rightarrow b\bar{b})$ (heavy flavor, 15k events), VBF $H(\rightarrow \tau\bar{\tau})$ (signal, 100k events). The samples are chosen as the kinematics are similar for Z and H VBF processes. In each case, the τ_h candidates were required to satisfy basic kinematical requirements such as: $p_T > 20$ GeV, $|\eta| < 2.1$, $m_{inv} < 3$ GeV, number of reconstructed particle composing the τ_h candidate to be less than 8, some energy deposit in the hadronic calorimeter (HCAL). Additional requirements are applied, based on the energy inside the isolation cone (see Figure 7), defined as the scalar sum of the tracks contained in the isolation cone ($0.10 < \Delta R < 0.40$) around the τ_h leading track.

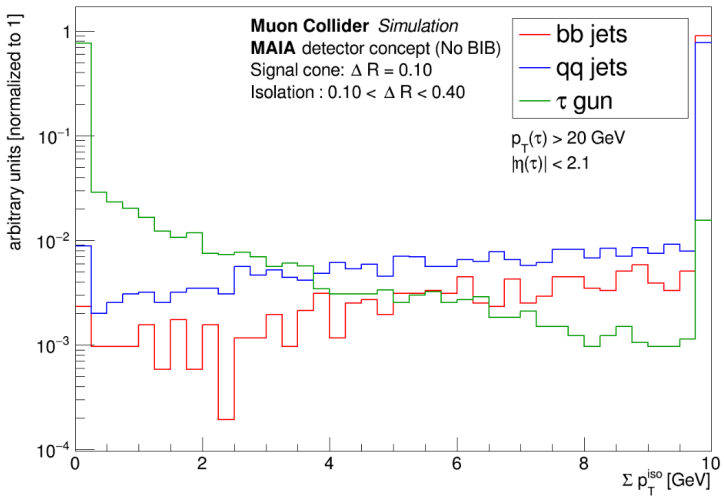

Figure 7. Distribution of the energy deposited in the isolation cone around the reconstructed τ_h candidates for different physics object samples. The isolation energy is a key variable used to suppress misidentified τs originating from hadronic jets, as genuine τs typically exhibit lower energy activity in the surrounding cone.

The misidentification rate is defined as the ratio between the number of reconstructed τ_h candidates and the total number of generated jet-like objects that have $p_T > 20$ GeV and $|\eta| < 2.1$. The τ_h efficiency is determined by calculating the ratio of reconstructed divided by the generated τ_h objects.

The results, reported in Table 2, indicate misidentification rates for light-flavored jets and for b-jets, separately. The τ_h reconstruction efficiency is also reported. In the case of electrons, fake τ_h candidates can arise when PandoraPFA misidentifies an electron as a charged hadron, since `TauFinder` only clusters the PF objects provided as input. This issue is addressed by requiring some energy deposition in the hadronic calorimeter, which effectively suppresses the misidentification of electrons as pions (Section 3.4.1). In contrast, the fake τ originate primarily from the difficulty in discriminating jets from genuine τ decays.

Table 2. Efficiency rates of various physics objects reconstructed as τ_h, after different requirements: kinematics, absolute ($E_{iso} < 3$ GeV) or relative ($E_{iso}/p_T^{lead} < 0.1$) leading track isolation. Rates are integrated over the full samples.

Physical Objects	**(u,s,d) Jets**	***b*-Jets**	τ_h
kinematics	13%	6%	69%
kin.+$E_{iso} < 3$ GeV	0.7%	0.1%	64%
kin.+$E_{iso}/p_T^{lead} < 0.1$	0.7%	0.1%	66%

The development of robust rejection techniques against fake τ_h implemented in this work is a first approach that can be further improved by dedicated studies, and it will be a key element of future `TauFinder` updates. In particular, further analyses of the misidentification rates as a function of p_T and η are required, and the implementation of a

multivariate approach, such as a boosted decision tree (BDT), to discriminate jets from real τ_h candidates will be an essential step toward achieving the performance needed for Higgs physics studies at a muon collider.

3.5. Tau Energy Reconstruction

When the visible products of the τ leptons interact with the detector, they are reconstructed with an energy that can differ from their true energy, due to both detector effects and statistical fluctuations. To correct for this bias, a dedicated study was performed using τ lepton particle-gun samples. In particular, the transverse momentum of the reconstructed visible decay products, $p_{T,\text{reco}}^{\text{vis}}$, was compared to the corresponding generator-level value $p_{T,\text{gen}}^{\text{vis}}$, for each decay mode. The resulting correlation for all hadronic τ decay modes is shown in Figure 8, although the energy correction parameters are obtained separately for each decay mode (1P0N, 1P1N, 3P), using dedicated linear fits such as:

$$p_{T,\text{gen}}^{\text{vis}} = a \cdot p_{T,\text{reco}}^{\text{vis}} + b$$

This correction ensures that the reconstructed kinematical distributions match more closely to the true ones, and it can be applied systematically to all τ_h candidates in the $H \to \tau_h\tau_h$ analysis. This study indicates that there is a good correlation between visible and generated τ_h energy values, with a resolution of 5-7%. Energy corrections are not deemed necessary and are not applied in this study.

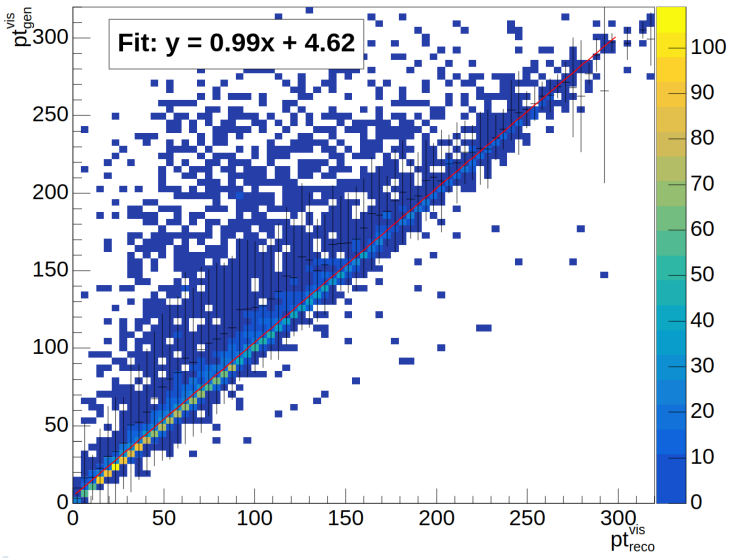

Figure 8. Correlation between reconstructed and generator-level transverse momentum of visible τ decay products in the τ-gun sample. The linear fit is used to derive the τ energy corrections.

4. Estimation of the Statistical Uncertainties on the Cross Section of the $H \to \tau^+\tau^-$ Process

The study of the $H \to \tau^+\tau^-$ decay provides direct sensitivity to the Higgs coupling to leptons, offering a powerful test of the SM and a probe for possible New Physics effects. This section focuses on the fully hadronic channel, $H \to \tau_h\tau_h$, reconstructed with the `TauFinder` algorithm described in Section 3. The analysis is performed in the context of a 10 TeV Muon Collider, with the goal of estimating the statistical precision on the cross section measurement. At this stage, the BIB is not yet included in the reconstruction, but preparatory cuts on transverse momentum and detector timing are applied to allow for its future integration.

4.1. Signal and Background Samples

The signal under study is the Higgs boson production via WW fusion at a 10 TeV Muon Collider, followed by its decay into a pair of τ leptons, $\mu^+\mu^- \to H\nu_\mu\bar{\nu}_\mu$, $H \to \tau^+\tau^-$ (Figure 9). The cross section for this process, as obtained from MadGraph5 at LO, is $\sigma = 52.17$ fb. Only the dominant WW fusion contribution is considered, while subleading production mechanisms such as ZZ fusion and Higgs-strahlung are neglected in this first study. SM parameters are used for all the generated samples in this study.

The main irreducible backgrounds are divided into three categories: (i) inclusive $\mu^+\mu^- \to \tau^+\tau^-\nu_\mu\bar{\nu}_\mu$ processes, with a total cross section of 127.4 fb, largely dominated by $\mu^+\mu^- \to Z\nu_\mu\bar{\nu}_\mu$, $Z \to \tau^+\tau^-$, (ii) vector boson scattering (VBS) diboson $\mu^+\mu^- \to W^+W^-(\to \tau^+\nu_\tau\tau^-\bar{\nu}_\tau)\nu_\mu\bar{\nu}_\mu$ and $\mu^+\mu^- \to W^+W^-(\to \tau^+\nu_\tau\tau^-\bar{\nu}_\tau)\mu\bar{\mu}$ processes, with a cross section of 16.1 fb, and (iii) $\mu^+\mu^- \to \tau^+\tau^-\mu^+\mu^-$ processes, with a cross section of 288.6 fb (Figure 10). In the latter

case, most of the final state muons are produced in the forward region outside the detector acceptance, making the visible final state indistinguishable from the signal. In this analysis, all type (ii) and (iii) processes are conservatively treated as background. The process in (ii) is found to be negligible, as the non-resonant $\tau\tau$ contribution is off-peak. Other backgrounds, such as $t\bar{t}$ and s-channel $\tau\tau$ production, are considered to be negligible. The samples generated at LO for the different processes, signal and background, are listed in Table 3.

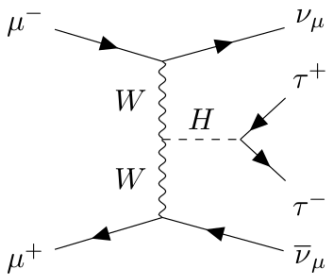

Figure 9. Feynman diagram of the $H \to \tau^+\tau^-$ signal process under investigation.

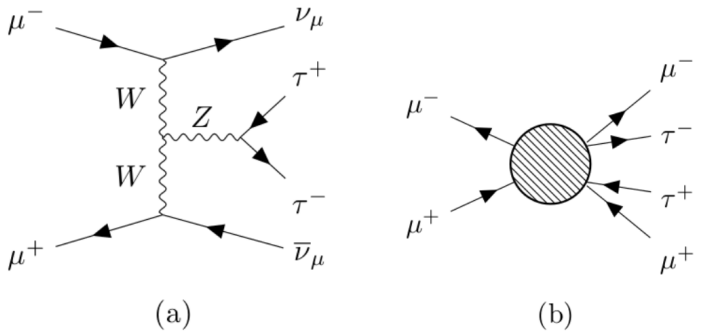

Figure 10. Feynman diagrams of the two main background processes in this analysis under investigation: (**a**) $\mu^+\mu^- \to Z\nu_\mu\bar{\nu}_\mu, Z \to \tau^+\tau^-$; (**b**) $\mu^+\mu^- \to \tau^+\tau^-\mu^+\mu^-$.

Table 3. Number of generated events and those that passed the selection, and the final efficiency ϵ for the signal and the main background processes, for an integrated luminosity of 10 ab^{-1}. Cross section values are extracted from Madgraph at LO.

Process	Details
$\mu^+\mu^- \to H\nu_\mu\bar{\nu}_\mu, H \to \tau^+\tau^-$	generated events: 100,000 ϵ = 0.06 σ = 52.17 fb expected events (10 ab^{-1}): 31,302
$\mu^+\mu^- \to Z\nu_\mu\bar{\nu}_\mu, Z \to \tau^+\tau^-$	generated events: 100,000 ϵ = 0.04 σ = 127.4 fb expected events (10 ab^{-1}): 50,960
VBS WW: $\mu^+\mu^- \to W^+W^-\nu_\mu\bar{\nu}_\mu, W^\pm \to \tau^\pm\nu_\tau$ $\mu^+\mu^- \to W^+W^-\mu^+\mu^-, W^\pm \to \tau^\pm\nu_\tau$	generated events: 10 000 ϵ = 0.05 σ = 16.1 fb expected events (10 ab^{-1}): 8050
$\mu^+\mu^- \to \tau^+\tau^-\mu^+\mu^-$	generated events: 100,000 ϵ = 0.01 σ = 288.6 fb expected events (10 ab^{-1}): 28,860

Backgrounds originating from fake τ_h candidates were not included at this stage, given the small misidentification rates observed in Section 3.4. However, they should be incorporated in future more complete studies.

4.2. Kinematical Variables

To characterize the kinematics of the reconstructed τ_h candidates and to identify possible differences between the signal and background processes, several observables were studied. Figure 11 shows the p_T distributions of the reconstructed τ_h candidates for signal and background samples.

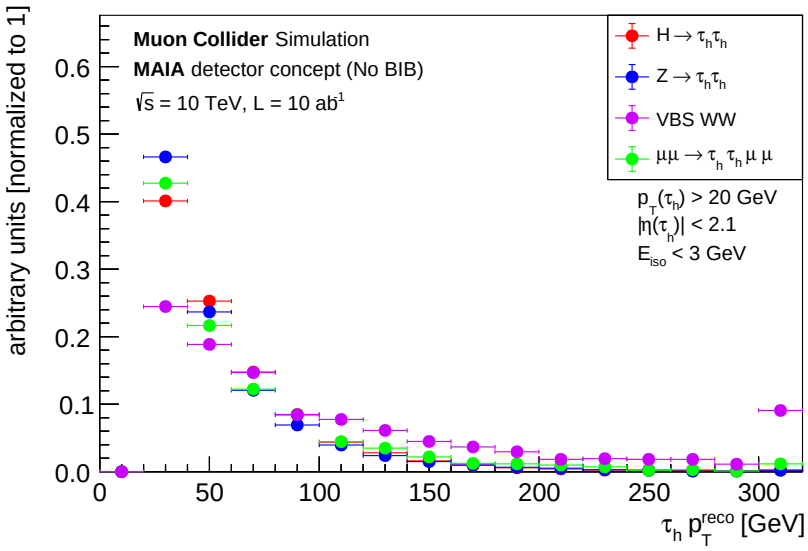

Figure 11. Transverse momentum distribution of the reconstructed τ_h candidates for the signal ($H \to \tau^+\tau^-$) and background samples ($Z \to \tau^+\tau^-$, VBS WW, and $\mu^+\mu^- \to \tau^+\tau^-\mu^+\mu^-$).

The pseudorapidity distributions of the reconstructed τ_h candidates are presented in Figure 12. Only τ_h within the detector acceptance, defined by $|\eta| < 2.1$, are considered in the analysis. This requirement ensures that the decay products are fully contained within the tracker and calorimeter systems.

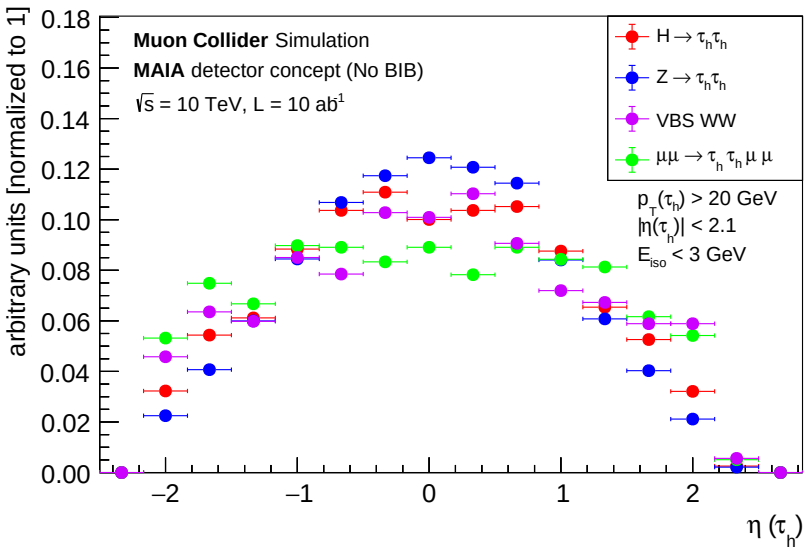

Figure 12. Pseudorapidity distribution of the reconstructed τ_h candidates for the three considered samples.

In addition, the angular separation ΔR between the two reconstructed τ_h candidates is shown in Figure 13. The distributions are distinctly different and could be used to further separate signal from backgrounds processes.

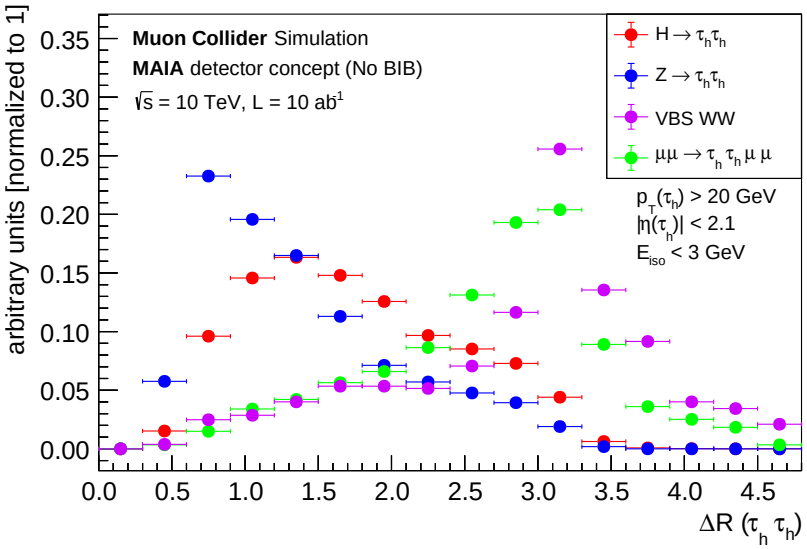

Figure 13. Distribution of the angular distance ΔR between the two reconstructed τ_h candidates for signal and background samples.

4.3. Event Selection

A simple event selection was performed by requiring the presence of exactly two oppositely charged reconstructed τ_h leptons (with either one or three reconstructed charged hadrons and no requirements on neutral particles). A pseudorapidity requirement of $|\eta| < 2.1$ is applied to the reconstructed τ_h candidates to ensure they fall within the detector acceptance region. A cut on the energy in the isolation cone of $E_{\text{iso}} < 3$ GeV is applied to select well-isolated τ_h candidates and suppress background contamination. In order to remove soft backgrounds, also in view of future inclusion of the soft particles from the BIB, a transverse momentum cut $p_{T,\text{reco}}^{\text{vis}} > 20$ GeV is required for the τ_h candidates. Some energy deposit in the HCAL is also required (Section 3.4.1). The efficiencies of the different samples after the event selection are reported in Table 3.

Such small efficiencies, despite the relatively mild selection requirements, can be explained by several factors. First, the shift of the reconstructed τ_h transverse momentum distribution towards lower values, due to the undetected neutrinos in the final state, leads to a loss of signal events when applying the p_T cut. The reconstruction efficiency of `TauFinder`, discussed in Section 3, also reduces the number of selected events. Finally, only about 42% (65% for each of the τ_h decays) of the signal events corresponds to the fully hadronic $\tau^+\tau^-$ final state considered in this study.

4.4. Fit Procedure and Results

The signal extraction is performed using the distribution of the visible invariant mass of the $\tau_h\tau_h$ system. The signal and background templates are obtained from the simulated samples after the full event selection and normalized to the expected integrated luminosity of 10 ab^{-1}. A binned maximum likelihood fit is then performed to the distribution of $m_{\tau_h\tau_h}^{\text{vis}}$, as illustrated in Figure 14. In the fit, the signal and background normalizations are left free to float and determined directly from the pseudo-data. The fitted signal yield is then converted into a measurement of the production cross section via

$$\sigma(H \to \tau_h\tau_h) = \frac{N_{\text{sig}}}{\epsilon \cdot L} \tag{2}$$

where N_{sig} is the number of fitted signal events, ϵ the total selection efficiency, and L the integrated luminosity.

The statistical uncertainty on the cross section is evaluated by generating pseudo-experiments in which the bin contents of the invariant mass distribution are varied according to Poisson statistics, and the fit procedure is repeated on each. The width of the distribution of fitted signal yields provides the estimate of the statistical error. The resulting relative statistical uncertainty on the cross section of the $H \to \tau_h\tau_h$ process is

$$\frac{\Delta\sigma}{\sigma} = 1.3\%.$$

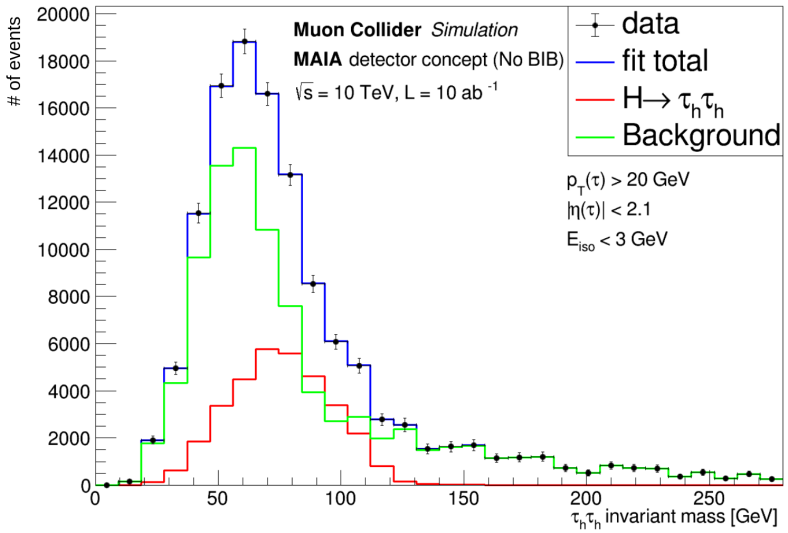

Figure 14. Fit of the visible invariant mass distribution of the $\tau_h\tau_h$ system at $\sqrt{s} = 10$ TeV for an integrated luminosity of 10 ab^{-1}. The black points represent the pseudo-data, while the red and green histograms show the fitted signal and background components, respectively. The background includes $\mu\mu \to Z\nu\bar{\nu}$, VBF diboson production and $\mu\mu \to \tau\tau\mu\mu$ processes (Table 3). The blue line is the total fit.

5. Discussion

A meaningful benchmark against which to compare our result is the projection of Ref. [22] obtained with `Delphes` [23] fast simulation at $\sqrt{s} = 10$ TeV for an equivalent integrated luminosity. The reported statistical precision on the $H \to \tau\tau$ cross section via W^+W^- fusion is $\Delta\sigma/\sigma = 1.1\%$, which is comparable to the result obtained in this work. The agreement indicates that our full simulation analysis yields a sensitivity comparable to the fast-simulation expectation. Both results are obtained without the inclusion of the BIB.

It is worth noting that a previous study at $\sqrt{s} = 3$ TeV with an integrated luminosity of $L = 1$ ab^{-1} for the $H \to \tau^+\tau^-$ channel at the Muon Collider [24] reported a statistical uncertainty of about 5.3%. The current analysis at $\sqrt{s} = 10$ TeV yields a relative statistical uncertainty of $\Delta\sigma/\sigma = 4.2\%$ for the same integrated luminosity, as shown in Figure 15. The results extrapolated to a total integrated luminosity of 20 ab^{-1}, corresponding to 10 ab^{-1} collected at each of the two anticipated interaction points, yield a relative statistical uncertainty of $\Delta\sigma/\sigma = 0.9\%$.

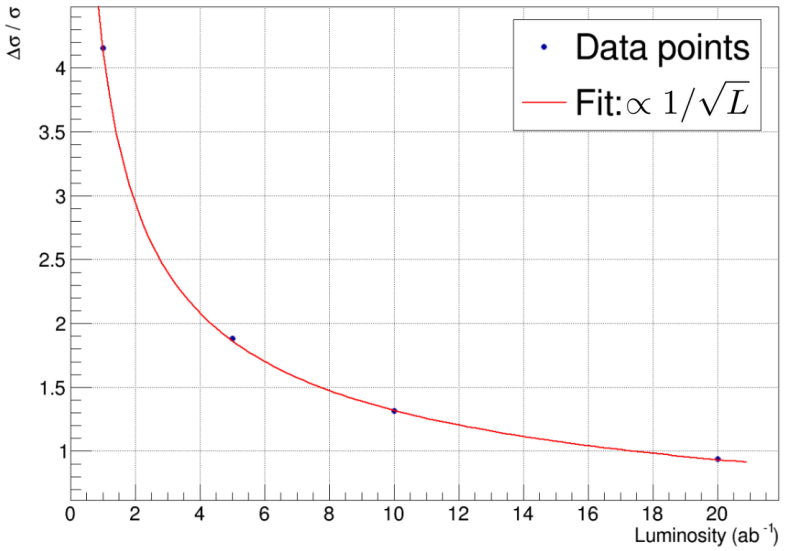

Figure 15. Expected relative statistical uncertainty on the $H \to \tau^+\tau^-$ cross section as a function of the integrated luminosity. $L = 20$ ab^{-1} corresponds to $L = 10$ ab^{-1} taken in each of the 2 predicted interaction points of a Muon Collider facility. For $L = 1$ ab^{-1}, the current result compares to a previous 3 TeV study (5.3%) [24].

Larger yields, higher center-of-mass energy, and an improved `TauFinder` algorithm used in this study help explaining the improved precision. Further improvements in the `TauFinder` algorithm are foreseen in the near future.

5.1. Beam Induced Background

A few consideration about the BIB. Although it was not included in the current study, the inclusion of the BIB is certainly important in a future sensitivity study to fully evaluate its impact. As the BIB is a machine-induced background from the decay of the muons circulating in the collider, the effects are mostly in the forward region. The BIB contribution is expected to be more forward at higher center-of-mass energies, i.e., 10 TeV compared to 3 TeV. Calorimeters are more affected than tracking detectors. One of the effects introduced by the BIB to the physical objects reconstruction is energy smearing. Previous studies [25] show that the jet energy resolution can go up from 5% to 20% in case of *b*-jets in the presence of BIB. As BIB affects the calorimeters more than the tracking, τs are expected to be less affected than (b-)jets. By applying a conservative smearing of 20% on the τ_h p_T, the fit in Figure 14 can be repeated and a relative uncertainty on the cross section of 1.5% is obtained, while a smearing of 10% yields an uncertainty of 1.4%.

It was demonstrated that the reconstruction algorithms can be optimized and improved to mitigate the effect of fake objects reconstructed from BIB particles, exploiting the fact that most of them are soft.

For example, fake jets from BIB can be suppressed by requiring the jets to contain at least one track with at least $p_T > 2$ GeV [25]. As such, we expect that the requirement on $p_T > 20$ GeV on τ_h will remove the majority of BIB contribution.

5.2. Comparison to Other Future Colliders

The current experimental precision on the coupling modifier κ_τ, as measured by the CMS [26] and ATLAS [27] collaborations, is still limited to about 8%. Looking ahead, the comparison can be extended to the projected sensitivities at other future colliders. The HL-LHC is expected to reach a precision on κ_τ of about 1.9%, while the FCC projections point to an ultimate precision of about 0.44% [28]. The result presented here, obtained at the 10 TeV Muon Collider, is therefore already competitive with the HL-LHC, and approaches the level of precision expected at the FCC. With further improvements in event reconstruction and in the dedicated $H \to \tau\tau$ analysis, the Muon Collider could thus provide a highly competitive measurement of the τ Yukawa coupling.

5.3. Future Improvements

Several improvements can be envisaged to enhance the sensitivity of the $H \to \tau\tau$ analysis at the Muon Collider. A first natural extension is the use of a multivariate technique such as a Boosted Decision Tree (BDT) to optimize the discrimination between signal and background. While in this work the signal extraction was based solely on the visible invariant mass of the $\tau_h\tau_h$ system, the addition of a BDT trained on angular and kinematic variables could significantly increase the signal-background separation.

A second improvement concerns the mitigation of jet–τ_h misidentification. A dedicated BDT could be trained to reduce the contribution of light- and *b*-jets misidentified as hadronic τs, thus further improving the purity of the selected sample.

Another important source of improvement is related to the τ reconstruction. In particular, the `TauFinder` algorithm can be optimized to better handle the cases where electrons or charged pions are misreconstructed as hadronic τs. In this analysis, this effect was only partially corrected by applying a cut on the energy deposit in the hadronic calorimeter, which proved effective in reducing the contamination from electron-like candidates. However, a more robust solution would require a dedicated revision of the algorithm, possibly including new identification variables.

Finally, an improvement in precision is expected by including other channels, both concerning the Higgs production (only VBF WW Higgs production was considered here, but VBF *ZZ* production and Higgstrahlung can also be considered) and visible final states by including events where at least one of the τs decays leptonically.

Overall, the implementation of advanced multivariate classifiers, together with a dedicated refinement of the τ reconstruction, has the potential to substantially improve the sensitivity to the $H \to \tau\tau$ process.

6. Conclusions and Outlook

The first full-simulation study of the $H \to \tau^+\tau^-$ process at a 10 TeV Muon Collider is presented, focusing on the fully τ hadronic decay channel. Using the `TauFinder` algorithm and a fit to the visible invariant mass, we obtain a relative statistical uncertainty on the cross section of

$$\frac{\Delta\sigma}{\sigma} = 1.3\%\ (0.9\%)\,,$$

for one (two) interaction point(s), comparable to `Delphes` projections. This demonstrates the robustness of the analysis with a realistic detector simulation, and highlights the competitive potential of the Muon Collider compared to the expectations at the HL-LHC and FCC that report sensitivities on the coupling modifiers of 1.9% and 0.44%, respectively [28].

Future improvements could further enhance the precision, in particular the use of multivariate techniques to improve signal–background separation, the inclusion in the analysis of more Higgs production modes and of the leptonic final states, refined τ lepton reconstruction to reduce τ_h misidentification, and the inclusion of beam-induced backgrounds. With these developments, the uncertainty on the $H \to \tau\tau$ cross section could be reduced well below the current result, confirming the Muon Collider as a unique facility for precision Higgs physics at the percent and sub-percent level.

Author Contributions

K.D., G.D.M., G.B.M. and L.V.: software, methodology, data analysis, investigation, original draft preparation, writing; M.G.: supervision, writing. All authors have read and agreed to the published version of the manuscript.

Funding

This research was partially funded by EU project "MuCol HORIZON-INFRA-2022-DEV-01-01" and Fundação para a Ciência e a Tecnologia (FCT), Portugal project 2024.00238.CERN.

Institutional Review Board Statement

Not applicable.

Informed Consent Statement

Not applicable

Data Availability Statement

Not applicable

Acknowledgments

Special thanks to Gregory Penn and Ethan Martinez, from Yale University, as well as Cyrus Kianian, Moses Glassman and Abdollah Mohammadi, from University of Wisconsin-Madison, for their collaboration and insights. We gratefully acknowledge the financial support provided by the EU project "MuCol HORIZON-INFRA-2022-DEV-01-01", the Fundação para a Ciência e a Tecnologia (FCT), Portugal.

Conflicts of Interest

The authors declare no conflict of interest.

Use of AI and AI-Assisted Technologies

No AI tools were utilized for this paper.

References

1. Higgs, P.W. Broken Symmetries and the Masses of Gauge Bosons. *Phys. Rev. Lett.* **1964**, *13*, 508.
2. Aad, G.; Abajyan, T.; Abbott, B.; et al. Observation of a new particle in the search for the Standard Model Higgs boson with the ATLAS detector at the LHC. *Phys. Lett. B* **2012**, *716*, 1–29.
3. Chatrchyan, S.; Khachatryan, V.; Sirunyan, A.M.; et al. Observation of a New Boson at a Mass of 125 GeV with the CMS Experiment at the LHC. *Phys. Lett. B* **2012**, *716*, 30–61.
4. Apollinari, G.; Brüning, O.; Nakamoto, T.; et al. High Luminosity Large Hadron Collider HL-LHC. *arXiv* **2015**, arXiv:1705.08830.
5. FCC Collaboration. FCC Physics Opportunities: Future Circular Collider Conceptual Design Report Volume 1. *Eur. Phys. J. C* **2019**, *79*, 474.
6. Abdallah, W.; Afanaciev, K.; Ahmad, S.; et al. CEPC Technical Design Report: Accelerator. *Radiat. Detect. Technol. Methods* **2024**, *8*, 1.
7. Bambade, P., Barklow, T., Behnke, T.; et al. The International Linear Collider: A Global Project. *arXiv* **2019**, arXiv:1903.01629.

8. Charles, T.K., Giansiracusa, P.J., Lucas, T.G.; et al. The Compact Linear Collider (CLIC)—2018 Summary Report. *arXiv* **2018**, arXiv:1812.06018.
9. Accettura, C., Adrian, S., Agarwal, R.; et al. Interim report for the International Muon Collider Collaboration (IMCC). *arXiv* **2024**, arXiv:2407.12450
10. Accettura, C.; Adams, D.; Agarwal, R.; et al. Towards a muon collider. *Eur. Phys. J. C* **2023**, *83*, 864.
11. Bell, C.; Calzolari, D.; Carli, C.; et al. MAIA: A new detector concept for a 10 TeV muon collider. *arXiv* **2025**, arXiv:2502.00181.
12. De Florian Sabaris, D.E.; Grojean, C.; Pieri, M.; et al. Handbook of LHC Higgs Cross Sections: 4. Deciphering the Nature of the Higgs Sector. *arXiv* **2016**, arXiv:1610.07922.
13. Taliercio, A.; Mastrapasqua, P.; Caputo, C.; et al. Higgs Self Couplings Measurements at Future proton-proton Colliders: a Snowmass White Paper. *arXiv* **2022**, arXiv:2203.08042.
14. Agostinelli, S., Allison, J., Amako, K.A.; et al. GEANT4—A Simulation Toolkit. *Nucl. Instrum. Meth. A* **2003**, *506*, 250.
15. ILCsoftware. Available online: https://ilcsoft.desy.de/portal/ (accessed on 23 January 2026).
16. Muon Collider. Software GitHub Folder. Available online: https://github.com/MuonColliderSoft (accessed on 23 January 2026).
17. Gaede, F. Marlin and LCCD: Software tools for the ILC. *Nucl. Instrum. Meth. A* 2006, 559, 177.
18. Marshall, J.S.; Thomson, M.A. The pandora particle flow algorithm. International Conference on Calorimetry for the High Energy Frontier. *arXiv* 2013, arXiv:1308.4537.
19. Navas, S.; Amsler, C.; Gutsche, T.; et al. Rev. Part. Phys. *Phys. Rev. D* **2024**, *110*, 030001.
20. Tumasyan, A., Adam, W., Andrejkovic, J.W.; et al. Identification of hadronic tau lepton decays using a deep neural network. *J. Instrum.* **2022**, *17*, P07023.
21. Muennich, A. *TauFinder: A Reconstruction Algorithm for τ Leptons at Linear Colliders*; CERN: Genève, Switzerland, 2010.
22. Forslund, M.; Meade, P. High precision Higgs from high energy muon colliders. *J. High Energy Phys.* **2022**, *8*, 185.
23. de Favereau, J.; Delaere, C.; Demin, P.; et al. DELPHES 3, A modular framework for fast simulation of a generic collider experiment. *J. High Energy Phys.* **2014**, *2*, 57.
24. Valla, L. *Higgs boson properties and tau lepton identification at the* $\sqrt{s}$ *= 3 TeV Muon Collider*; CERN: Genève, Switzerland, 2024.
25. Andreetto, P.; Casarsa, M.; Gianelle, A.; et al. Higgs Physics at a 10 TeV Muon Collider with the MUSIC Detector. PoS EPS-HEP2025 385. In Proceedings of the European Physical Society Conference on High Energy Physics (EPS-HEP2025), Marseille, France, 7–11 July 2025.
26. The CMS Collaboration. A portrait of the Higgs boson by the CMS experiment ten years after the discovery. *Nature* **2022**, *607*, 60.
27. The ATLAS Collaboration. A detailed map of Higgs boson interactions by the ATLAS experiment ten years after the discovery. *Nature* **2022**, *607*, 52.
28. De Blas, J.; Cepeda, M.; D'Hondt, J.; et al. Higgs Boson Studies at Future Particle Colliders. *J. High Energy Phys.* **2020**, *2020*, 139.